SECURITY INFORMATION

Copy 241
RM E53I24

NACA RM E53I24

TECH LIBRARY KAFB, NM
0144273

6842

NACA

RESEARCH MEMORANDUM

INVESTIGATION OF A HIGH-PRESSURE-RATIO EIGHT-STAGE AXIAL-FLOW RESEARCH COMPRESSOR WITH TWO TRANSONIC INLET STAGES

I - AERODYNAMIC DESIGN

By Charles H. Voit

Lewis Flight Propulsion Laboratory
Cleveland, Ohio

CLASSIFIED DOCUMENT

This material contains information affecting the National Defense of the United States within the meaning of the espionage laws, Title 18, U.S.C., Secs. 793 and 794, the transmission or revelation of which in any manner to an unauthorized person is prohibited by law.

NATIONAL ADVISORY COMMITTEE
FOR AERONAUTICS

WASHINGTON

December 4, 1953

RECEIPT SIGNATURE
REQUIRED

TECH LIBRARY KAFB, NM
0143273

NATIONAL ADVISORY COMMITTEE FOR AERONAUTICS

RESEARCH MEMORANDUM

INVESTIGATION OF A HIGH-PRESSURE-RATIO EIGHT-STAGE AXIAL-FLOW RESEARCH COMPRESSOR WITH TWO TRANSONIC INLET STAGES

I - AERODYNAMIC DESIGN

By Charles H. Voit

3018

T-SO

SUMMARY

An eight-stage high-pressure-ratio axial-flow compressor was designed for use as a research unit in which the problems associated with design and off-design performance of transonic stages combined with highly loaded subsonic stages could be studied. This compressor consisted of two transonic inlet stages and six subsonic stages designed to produce an over-all total-pressure ratio of 10.26 with a mass flow of 29.8 pounds per square feet of rotor frontal area at a tip speed of 1168 feet per second. The transonic inlet stage was designed without guide vanes for an axial inlet and a maximum relative Mach number of 1.20. The subsonic stages were designed for somewhat higher loading limits in the middle stages than in the latter stages. The tip diameter of the compressor was 20 inches and the inlet hub-tip ratio at the entrance to the first rotor was 0.48.

This report discusses the design procedure and presents the experimentally determined over-all performance of this compressor.

INTRODUCTION

Compactness and reduced weight of axial-flow compressors for gas-turbine power plants in aircraft application can best be achieved by: (1) decreasing the compressor length by reducing the number of stages required to produce the desired pressure ratio; and (2) decreasing the compressor diameter by increasing the mass flow per unit frontal area while, at the same time, maintaining high efficiencies. Two-dimensional high-speed cascade data (ref. 1) and single-stage rotor tests (refs. 2 and 3) indicate that higher stage pressure ratios than those currently being used are obtainable with the use of high blade loading and high subsonic Mach numbers while maintaining good efficiencies.

The compressor of reference 4 was built and tested in order to investigate the possibility of staging highly loaded stages and to study

the problems associated with highly loaded multistage compressors. This compressor showed that it is possible to increase the stage pressure ratios above those currently being used while maintaining good mass flow per unit frontal area and acceptable efficiencies (ref. 5). The compressor of reference 4 was designed for an average stage pressure ratio of 1.205 and a weight flow of 26.4 pounds per unit frontal area. Although this is a comparable weight flow and a higher stage loading than most current commercial designs, it is conservative compared with the obtainable values as indicated by analysis of cascade and single-stage data.

In order to investigate the problems associated with even higher stage pressure ratios and high over-all pressure ratios, a completely subsonic multistage compressor design was made, on the basis of the analysis of reference 6, to produce an over-all pressure ratio of 10.3 in nine stages, an average stage pressure ratio of 1.296, with an equivalent weight flow of 26.5 pounds per square foot of frontal area. Shortly after this design was completed and its fabrication started, the performance of a single-stage transonic research compressor was determined (ref. 7). This transonic stage utilized high rotor-tip relative Mach numbers, of the order of 1.1, which permitted high stage pressure ratios and high weight flows and gave good efficiencies and a wide efficient operating range.

In order to take advantage of the desirable characteristics indicated for the transonic stage, and because it was believed that the subsonic inlet design might have poor off-design characteristics because of the high guide-vane turning required and consequently the high rotor-tip static-pressure rise, the first two stages were redesigned to transonic stages. An attempt was made to replace only the first subsonic stage with a transonic stage. However, in order to reduce the supersonic Mach number entering the first rotor tip to a subsonic value of 0.80 entering the second stage, a first-stage stator having a reversal of twist between hub and tip would be required. This reversal was believed to be undesirable and, hence, the first two stages were redesigned. The resulting nine-stage transonic inlet compressor design gave an over-all pressure ratio of 13.5. Because such a high pressure ratio might be beyond the practical limit in a single-spool compressor, only the first eight stages, which had an over-all pressure ratio of 10.26, were built. However, the mechanical design is such that the ninth stage can be added later if desired.

The Mach number and stage loading limits were increased above those employed in the design of the compressor of reference 4 to values which were believed to be near the practical limit. The high stage pressure ratios were obtained by using high rotative speeds with moderate turning angles. The resulting compressor design, which is discussed herein, was made in order to study the design and off-design performance problems of a multistage compressor with high mass flow, high stage pressure ratio, and high over-all pressure ratio. This compressor design, therefore,

3018

provides a research unit in which to study not only the effect of high blade loading and high over-all pressure ratio but also the performance of transonic stages in a multistage compressor.

SYMBOLS

The following symbols are used in this report:

A	rotor frontal area, sq ft
a	local speed of sound, ft/sec
b	blade chord, in.
C_L	lift coefficient
$C_{L,i}$	design camber (theoretical C_L of isolated airfoil)
c_p	specific heat of air at constant pressure, Btu/(lb)(^oR)
c_v	specific heat of air at constant volume, Btu/(lb)(^oR)
D	diffusion factor across stator row
D'	diffusion factor across rotor row
g	acceleration due to gravity, 32.174 ft/sec^2
h	dimensionless ratio of axial component of air velocity to rotor tip speed, V_a/U_t
i	incidence angle, deg
M	absolute Mach number
M'	Mach number relative to rotating blades
n	polytropic exponent of compression
P	total or stagnation pressure, lb/sq ft
ΔP	change in absolute pressure, lb/sq ft
q	velocity head $V^2/2g$, ft
R	radius of circular-arc blade section, in.
r	radius of compressor, ft
T	total or stagnation temperature, ^oR

[redacted]

t	maximum blade thickness, in.
U_t	velocity of rotor blade at tip, ft/sec
$U_t/\sqrt{\theta}$	equivalent blade tip speed corrected to standard NACA sea-level conditions, ft/sec
V	absolute air velocity, ft/sec
V'	air velocity relative to rotating blades, ft/sec
$\frac{W\sqrt{\theta}}{\delta}$ or W	equivalent weight flow corrected to standard NACA sea-level conditions, lb/sec
X	ratio of absolute tangential velocity to rotor tip speed
Y	ratio of change in tangential velocity through stator to rotor tip speed
Y'	ratio of change in tangential velocity through rotor to rotor tip speed
Z	ratio of blade speed at any radius to blade tip speed, or radius ratio r/r_t
β	angle between absolute velocity vector and rotor axis, deg
β'	angle between relative velocity vector and rotor axis, deg
$\Delta\beta$	absolute turning angle through stator, deg
$\Delta\beta'$	relative turning angle through rotor, deg
γ	ratio of specific heats, c_p/c_v, 1.3947
δ	ratio of total pressure to standard NACA sea-level pressure
δ°	deviation angle, deg
η	adiabatic temperature-rise efficiency
θ	ratio of total temperature to standard NACA sea-level temperature
ρ	mass density of air, slugs/cu ft
σ	blade-element solidity, chord/spacing

3018

φ	camber angle of circular-arc blade section (included angle of mean line), deg
ψ	angle between blade chord and compressor axis, deg

Subscripts:

a	axial direction
e	simple radial equilibrium
h	hub
m	mean
n	any station
s	static or free-stream conditions
ss	subsonic stages
T	total or stagnation conditions
t	tip
ts	transonic stages
W	straight-through flow
0	compressor-inlet stagnation conditions, standard NACA sea-level conditions
1,3,5, . . . 15	stations ahead of rotor of 1st, 2nd, 3rd, . . . 8th stages
2,4,6, . . . 16	stations ahead of stator of 1st, 2nd, 3rd, . . . 8th stages
20	discharge measuring station

PRELIMINARY DESIGN CONSIDERATIONS AND LIMITATIONS

The original subsonic compressor was designed to produce as high an average stage pressure ratio as possible with good efficiency. In order to obtain good efficiency, certain design limits were imposed. These

design limits were a Mach number limit and blade-loading limits. The multistage analysis of reference 6 indicates that there is a certain desirable stagewise distribution of axial velocity and relative inlet air angle that will permit the highest stage pressure ratio without exceeding the prescribed Mach number and blade-loading limits. The method of reference 6 was therefore used to determine the stagewise distribution of tip axial velocity, tip relative inlet air angle, and stage total-pressure ratio.

The subsonic design used a Mach number limit of 0.8 on the basis of the results of references 2 and 3. Above a Mach number of 0.8 the total-pressure loss coefficient for 65-series blower blade sections, with a thickness from 6 to 10 percent of chord, increases sharply with Mach number.

The blade-loading limits were those used in the analysis of reference 6, that is, σC_L, $\Delta P_s/q_a$, and $\Delta\beta_t'$. The method of applying these limits and the numerical values used are given in the section "Stagewise distribution of design variables."

Recently, a more satisfactory limiting-blade-loading parameter has been developed (ref. 8). This derived limiting diffusion factor comprises a term involving the velocity ratio across the blade and a term proportional to the circulation about the element, and is given by

$$D' = \left(1 - \frac{V_{n+1}'}{V_n'}\right) + \frac{Y'U_t}{2\sigma V_n'}$$

and

$$D = \left(1 - \frac{V_{n+2}}{V_{n+1}}\right) + \frac{YU_t}{2\sigma V_{n+1}}$$

For a given inlet air angle, $\Delta P_s/q_a$ is proportional to the first term, and σC_L and $\Delta\beta'$ are functions of the second term of the diffusion factor. Reference 8 gives a correlation between this diffusion factor and σC_L and $\Delta\beta'$ for 65-series cascade and single-stage compressor data. Although this limiting-blade-loading parameter was not used in this design, the numerical value of the diffusion factor for hub, mean, and tip radii of each blade row is presented in table II for the reader's information.

3018

DESIGN OF SUBSONIC STAGES

Inlet stage. - Even though it was later discarded, the original subsonic inlet stage design will be discussed briefly, because its characteristics affect the final design. The subsonic inlet design determined the equivalent weight flow and equivalent tip speed of the latter stages, which had to be maintained when the inlet stages were redesigned to transonic stages. The subsonic inlet stage design also set the starting point for determining the stagewise distribution of stage pressure ratio, tip dimensionless axial velocity, and tip relative inlet air angle (see fig. 1) and hence affected the latter stages.

The subsonic inlet stage design was very similar to that chosen for the multistage analysis of reference 6 with slight modifications due to the higher hub-tip ratio (0.55) of this compressor. The subsonic-inlet-stage design total-pressure ratio was 1.189 with an equivalent weight flow of 26.5 pounds per square foot of rotor frontal area at an equivalent tip speed of 1120 feet per second. The tip relative inlet air angle was set at 60° and the resulting tip dimensionless axial velocity h_t was 0.3855.

Stagewise distribution of design variables. - The stagewise distribution of tip dimensionless axial velocity h_t, relative rotor-tip inlet air angle β_t', and stage total-pressure ratio were determined by methods similar to those used in reference 6. Reference 6 indicates that there is a certain desirable stagewise distribution of axial velocity which will permit a high stage pressure ratio without exceeding the design limits used. This distribution is a steadily increasing axial velocity. Because this distribution results in high discharge velocities and small passage height, and because reference 6 indicates that some deviation from the optimum distribution could be tolerated without a great sacrifice in stage pressure ratio, the present design maintained the tip axial Mach number entering each rotor row approximately constant. By use of the method of reference 6, the tip axial velocities at a midstage, where the over-all total-pressure ratio equals 3, and at a latter stage, where the over-all total-pressure ratio is 9, were calculated so that the tip axial Mach numbers were approximately constant. Total temperatures were used in this calculation because the static temperatures cannot be determined, since the velocities are not known at these stations. This results in a somewhat higher axial velocity than would be obtained if static temperatures were used. With the use of these tip axial velocities, a given set of design limits, and the curves of reference 6, the relative tip inlet air angles and stage total-pressure ratio were determined. The limits used were σC_L, 1.2; $\Delta P_s/q_a$, 1.6; and $\Delta\beta_t'$, 22° for the midstage; and σC_L, 1.0; $\Delta P_s/q_a$, 1.6; and $\Delta\beta_t'$, 20° for the latter stage. The inlet-, midstage, and latter-stage values of tip dimensionless axial

velocity, stage total-pressure ratio, and tip relative inlet air angle were plotted on semilog coordinates and smooth curves were faired (fig. 1). With the use of this stage total-pressure ratio distribution, the over-all total-pressure ratio entering each succeeding stage was calculated, and the values of h_t and β_t' entering each stage and the total-pressure ratio for each stage were determined from the faired curves. The discharge axial velocities thus determined were believed to be too high for efficient use in jet-engine application, and it was decided to limit the dimensionless tip axial velocity ratio of the last three stages to 0.50. The values of h_t, β_t', and the stage pressure ratio used for the subsonic design are given in table I.

3018

Efficiency assumption. - It is necessary to assume efficiencies for each stage in order to determine the energy addition necessary for the desired stage total-pressure ratio. These assumed efficiencies are given in table I. The efficiencies assumed for the first two subsonic stages were somewhat lower than the middle stages because inlet stages with low hub-tip ratios usually have low efficiencies because of high rotor-tip diffusion and low solidities. The efficiencies of the exit stages were also assumed somewhat lower than the middle stages because the boundary layer and the tip clearance were believed to be a greater percentage of the passage height, and both of these factors tend to increase the losses in the latter stages and decrease the efficiency.

Velocity diagrams. - With the desired values of tip dimensionless axial velocity, tip relative inlet air angle, stage total-pressure ratio, and an assumed stage efficiency known for each stage, it is possible to determine the velocity diagram at any radius if the radial variation of tangential velocity entering a rotor, the change in tangential velocity through the rotor, and the radial variation of axial velocity are assumed. The tangential velocity entering any rotor row was assumed to vary directly with radius, and the change through the rotor varied inversely with radius. The variation of the axial velocity entering any rotor row was calculated by assuming the existence of simple radial equilibrium (no radial flow or radial entropy gradient) and constant total enthalpy along the radius. The variation of the axial velocity entering any stationary row was assumed to be the average between that required for simple radial equilibrium and that required for straight-through flow (straight-through flow, as used herein, is defined as no change in the radial distribution of the axial velocity entering and leaving a blade row). Single-stage data available at the time the design was made indicated that this type of axial-velocity distribution is obtained after a rotor row (ref. 9, fig. 7). More recent investigations indicate that nonisentropic simple radial equilibrium, which considers the radial variation of entropy, is very nearly obtained after a rotor-blade row.

With these assumptions and the values given in table I, the components of the velocity diagram can be calculated at any radius. Details

of these calculations are given in the section Design Calculation Method. The components of the velocity diagrams entering and leaving a blade row were calculated at the same radius. This calculation assumes that the flow is along cylinderical surfaces across a blade row. The tangential velocity component leaving the last-stage stators was removed by a row of exit guide vanes in order to have axial discharge from the compressor.

Flow-passage geometry. - After the radial variation of the velocity diagrams is determined, the hub profile is determined. The hub radius entering each blade row can be determined from continuity and the flow conditions at that station. It is then necessary to fix the axial length of the blade rows and the clearance between them in order to determine the hub profile. The casing of the compressor of reference 4 was used, and hence the axial spacing of the stator blades was fixed, which in turn determined the axial spacing of the rotor-blade rows because the clearance between blade rows could not be altered appreciably. The resulting hub profile was slightly wavy, and a smooth curve was faired for the hub profile. The faired hub contour deviated only very slightly from the calculated points, and this procedure was believed justified because the boundary-layer allowance was not known to a high degree of accuracy.

Boundary-layer allowance. - The hub-contour determination described in the preceding section did not make any allowance for boundary layer along the passage walls. In order to make some allowance for boundary layer, the passage height was increased by decreasing the hub radii by an amount equal to the estimated displacement thickness of the combined outer- and inner-wall boundary layers. Very little information could be obtained on the probable thickness of the boundary layers. Based on the best available information, the stagewise distribution of boundary-layer thickness shown in figure 2 was assumed. This distribution assumed a zero thickness at the inlet to the first rotor, a linearly increasing thickness through the fourth stage, and a constant thickness for the remaining stages. More recent data indicate that this boundary-layer allowance may have been excessive in the latter stages, which would result in the latter stages being excessively loaded and their design-speed operation being nearer stall than was intended in the design. A sketch of the flow passage and blading is given in figure 3.

DESIGN OF TRANSONIC STAGES

When the performance of the transonic compressor of reference 7 became known, it appeared highly desirable to incorporate transonic inlet stages into this multistage design. A completely new design with transonic inlet stages would have been more desirable, but this was not feasible because fabrication of the subsonic design had already begun and it was necessary to keep all changes, both aerodynamic and mechanical, to a minimum. The first two stages were therefore redesigned and the other

stages remained unchanged. In order to do this the first two stages were so designed that both the magnitude and the radial distribution of flow angles and equivalent velocities $V/\sqrt{\theta}$ leaving the second transonic stage were identical with those of the subsonic design. These conditions placed some restrictions on the design of the two transonic stages.

In order to keep the flow velocities entering the third stage identical with those of the original subsonic design, the same equivalent weight flow $W\sqrt{\theta}/\delta$ and equivalent tip speed $U_t/\sqrt{\theta}$ were maintained at the entrance to the third stage. Because the pressure ratio and temperature ratio across the transonic stages are higher than the original subsonic stages, it was possible to increase the entrance weight flow and necessary to increase the design tip speed. In order to obtain equivalent velocities entering the third stage it was necessary that

$$W_{ts}\left(\frac{\sqrt{T_5/T_0}}{P_5/P_0}\right)_{ts} = W_{ss}\left(\frac{\sqrt{T_5/T_0}}{P_5/P_0}\right)_{ss}$$

then

$$W_{ts} = W_{ss}\left(\frac{\sqrt{T_5/T_0}}{P_5/P_0}\right)_{ss}\left(\frac{P_5/P_0}{\sqrt{T_5/T_0}}\right)_{ts}$$

$$= W_{ss}\left(\frac{\sqrt{T_5/T_0}}{P_5/P_0}\right)_{ss}\left(\frac{P_5}{P_0}\right)_{ts}^{\frac{n+1}{2n}}$$

Hence, in order to maximize the weight flow, it would be desirable to obtain as high a pressure ratio across the transonic stages as possible. However, for a given entrance annulus area, increasing the weight flow increases the axial Mach number; and for a rotor with axial inlet, the relative Mach number is also increased. These relations are given by the following equations:

$$\left(\frac{P_5}{P_0}\right)_{ts}^{\frac{n+1}{2n}} = \left[\pi(r_t^2 - r_h^2)_1 \rho_0 \frac{\rho_1}{\rho_0} g M_{a,1} a_0 \frac{a_1}{a_0}\right]_{ts} \frac{1}{W_{ss}\left(\frac{\sqrt{T_5/T_0}}{P_5/P_0}\right)_{ss}}$$

3018

$$U_{t,ts} = U_{t,ss} \frac{(T_5/T_0)_{ts}^{\frac{1}{2}}}{(T_5/T_0)_{ss}^{\frac{1}{2}}} = U_{t,ss}\left(\frac{T_5}{T_0}\right)_{ss}^{-\frac{1}{2}}\left(\frac{P_5}{P_0}\right)_{ts}^{\frac{n-1}{2n}}$$

$$M'_{1,t} = \left[M^2_{a,1,t} + \left(\frac{U_t}{a_1}\right)^2\right]^{\frac{1}{2}}_{ts}$$

where the superscript n represents the polytropic exponent of compression.

For given values of $W_{ss}\left(\frac{\sqrt{T_5/T_0}}{P_5/P_0}\right)_{ss}$, r_t, r_h, and n, the pressure ratio, tip speed, and relative tip Mach number can be determined as a function of the axial Mach number. The term $W_{ss}\left(\frac{\sqrt{T_5/T_0}}{P_5/P_0}\right)_{ss}$ was fixed by the original subsonic design, the tip radius was fixed by the casing of the compressor of reference 4 at 10 inches, and the hub radius entering the first rotor could not be reduced below 4.8 inches because of the existing inlet bearing support geometry. With these values and an assumed polytropic efficiency of 0.88 for the transonic stages and with the relative Mach number entering the first rotor at the tip limited to 1.20, the following design values were obtained for the transonic stages:

Axial Mach number entering first rotor	0.534
Total-pressure ratio across transonic stages	1.888
Equivalent weight flow, lb/sec	65
Equivalent weight flow per unit rotor frontal area, (lb/sec)/sq ft	29.8
Equivalent tip speed, ft/sec	1168

The Mach number limit of 1.20 was based on single-transonic-stage data available at that time.

The total-pressure ratio was divided between the two stages with each having a total-pressure ratio of 1.374. Constant energy addition from hub to tip was used in the transonic stages because the subsonic stages were designed for no radial energy gradient, and it would be impossible to match the design flow entering the subsonic third stage if the first two stages were designed for a radial energy gradient. In order to match the design flow angles entering the third stage, it was necessary for the first two stator rows to change the tangential velocity

added by the first two rotors to that required at the entrance of the third stage of the subsonic design. The stator of the first transonic stage was designed to produce a constant tangential velocity radially at the exit of the first stage. This reduced the amount of change in tangential velocity necessary in the second stator at the hub, as well as reducing the relative Mach number entering the second rotor. The second stator row then changed the tangential velocity after the second rotor to that required by the subsonic design at the entrance to the third stage. The radial variation of axial velocity after each blade row of the transonic stages was calculated from simple radial equilibrium and constant total enthalpy along the radius. The velocity diagram at hub, mean, and tip for the transonic stages are given in figure 4 and the design values for all stages in table II.

3018

MECHANICAL CONSIDERATIONS

In this compressor design it was desired to use as many of the existing parts of the compressor of reference 4 as possible without compromising the design, especially the inlet and outlet parts which house the bearing assemblies and the outer casing. The use of the outer casing made it impossible to increase appreciably the solidity of the subsonic stator blades because the number of blades and the axial space available were fixed. The solidity of these stator blades is somewhat lower than would be desirable for highly loaded stages. The existing rotor of the compressor of reference 4 could not be used because the hub contour was unsuitable for this design, and the number of blade slots and hence the solidity of the rotor rows were too low for highly loaded stages.

A number of changes was necessitated by incorporating the transonic inlet stages into the design. The hub-tip ratio at the entrance to the first stage was decreased from 0.55 to 0.48 in order to utilize the high pressure ratio obtainable with the transonic stages and still match the equivalent flow entering the first subsonic stage and not exceed the limiting relative Mach number at the tip of the first rotor.

The transonic stages were believed to require larger blade chords than the subsonic stages and hence it was necessary to alter the original axial location of the subsonic blade rows in order to obtain the necessary axial space for the transonic stages. More recent data indicate that good performance can be obtained with lower solidities. However, because the transonic stages were designed for a higher pressure ratio than the subsonic stages which they replaced, the over-all pressure ratio remained approximately the same for the eight stages as it was for the original nine subsonic stages. The greater mass flow of the transonic design and a desire not to increase the exit velocitites at station 20

(fig. 3) necessitated increasing the exit-flow area. This was done by increasing the outer radius downstream of the exit guide vanes.

DESIGN CALCULATION METHOD

Subsonic design. - The design of the subsonic stages was based on the analysis of reference 6 and was carried out by selecting a stagewise distribution entering each rotor of tip dimensionless axial-velocity ratio h_t, tip relative inlet air angle β_t', stage total-pressure ratio, and stage polytropic efficiency. These values are given in table I. The tip speed and weight flow are set by the first stage. With the tip inlet air angle, tip axial velocity, and over-all pressure and temperature ratio entering any stage known, the velocity diagram and the passage height at the entrance to each stage can be calculated by the following equations. (The subscript n indicates any axial station entering a rotor, n + 1 is entering the following stator, and n + 2 is leaving the stators.) The tangential velocity at the tip entering any rotor can be determined by the equation

$$X_{n,t} = 1.0 - h_{n,t} \tan \beta'_{n,t}$$

and at any radius by

$$X_n = X_{n,t} Z_n$$

since wheel-type flow is specified leaving each stator row. The axial-velocity ratio at any radius is given by

$$h_n^2 = \left[h_{n,t}^2 + 2X_{n,t}^2 (1 - Z_n^2) \right]^{\frac{1}{2}}$$

which assumes simple radial equilibrium. The ratio of static to total density at any radius is

$$\left(\frac{\rho_s}{\rho_T} \right)_n = \left[1 - \frac{\gamma - 1}{2} \frac{U_t^2}{a_0^2} \frac{1}{T_n/T_0} (h_n^2 + X_n^2) \right]^{\frac{1}{\gamma - 1}}$$

The total temperature entering any stage can be determined from the scheduled stage total-pressure ratios and assumed stage efficiencies. The weight-flow equation is

$$W = 2\pi r_t^2 g \rho_0 (\rho_T/\rho_0)_n U_t \int_{(Z_h)_n}^{1.0} (\rho_s/\rho_T)_n h_n Z_n \, dZ_n$$

The value of ρ_T/ρ_0 at any station n can be found from the scheduled stage pressure ratios and efficiencies. All terms inside the integral can be calculated for various values of Z and the integral evaluated. The lower limit Z_h is then adjusted until the correct value of weight flow is obtained. This procedure determines the hub radius, uncorrected for boundary layer, entering each rotor row. The axial and tangential velocity components and wheel speed entering any rotor can be determined from the preceding equations and hence both absolute and relative flow velocities, flow angles, and Mach numbers can be determined.

3018

The calculations of the flow leaving a rotor row are done in a similar manner except for the radial distribution of axial velocity. For this design the radial variation of axial velocity after subsonic rotor rows was assumed to be the average of that required for simple radial equilibrium and that for straight-through flow. Because the axial velocity increased across a stage, the radial variation of axial velocity for straight-through flow was assumed to be the average of that entering a rotor row and that leaving the next stator row.

The dimensionless change in tangential velocity Y' across a rotor row was calculated from the scheduled total-pressure ratio and efficiency for each stage according to the following equation:

$$Y'_t = \left[\left(\frac{P_{n+2}}{P_n}\right)^{\frac{n-1}{n}} - 1\right]\frac{T_n/T_0}{(\gamma-1)\left(\frac{a_0}{U_t}\right)^2}$$

where the superscript n represents the polytropic exponent of compression. The variation of Y' with radius is

$$Y' = Y'_t/Z$$

The tangential velocity leaving a rotor row is

$$X_{n+1} = X_n + Y'$$

The axial velocity after a rotor row at any radius for straight-through flow is

$$h_{n+1,W} = \frac{h_n + h_{n+2}}{2}$$

The axial-velocity variation for simple radial equilibrium after a rotor row is

$$h_{n+1,e} = \left[h_{n+1,m,W}^2 - 2X_{n,t}^2 (Z^2 - Z_m^2) - 4X_{n,t} Y_t \ln \frac{Z}{Z_m} \right]^{\frac{1}{2}}$$

The design axial-velocity variation after a rotor row at any radius is

$$h_{n+1} = \frac{h_{n+1,e} + h_{n+1,W}}{2}$$

The ratio of static to total density is

$$\left(\frac{\rho_s}{\rho_T} \right)_{n+1} = \left[1 - \frac{\gamma - 1}{2} \left(\frac{U_t}{a_0} \right)^2 \frac{1}{\frac{T_{n+1}}{T_0}} (h_{n+1}^2 + X_{n+1}^2) \right]^{\frac{1}{\gamma - 1}}$$

and the weight-flow equation is

$$W = 2\pi r_t^2 g \rho_0 (\rho_T / \rho_0)_{n+1} U_t \int_{Z_{h,n+1}}^{1.0} (\rho_s / \rho_T)_{n+1} h_{n+1} Z_{n+1} \, dZ_{n+1}$$

The value of the lower limit of the integral $Z_{h,n+1}$ is adjusted to give the correct weight flow, thus determining the hub radius after each row.

The values of Z_h determined by the preceding procedure plotted with the axial spacing required by existing parts resulted in a slightly wavy hub profile, and the actual hub profile used was obtained by fairing a smooth curve through the calculated points.

Transonic stages. - The velocity-diagram calculation for the transonic stages was made in the same manner with the following exceptions:

(1) The radial variation of axial velocity after each blade row was assumed to be that required for simple radial equilibrium.

(2) Flow conditions entering and leaving a blade row were calculated along an assumed streamline, rather than at a constant radius, because of the large changes in hub radii of these stages. The streamlines were assumed to pass through the area centers of five equal-area increments at each station.

3018

(3) The hub radius at each station was adjusted to produce a smooth hub profile by a trial-and-error adjustment of the axial velocities at each station.

(4) The tangential velocity component leaving the stators was not wheel type.

(5) In calculating the energy addition through the rotors, the change in radii of the flow across the rotor was taken into account and hence the change in tangential velocity is not a vortex as was assumed in the subsonic stages.

3018

BLADE SELECTION

Transonic blades. - The blade sections used for the transonic rotor blades were composed of circular-arc pressure and suction surfaces and had a circular-arc mean line. These sections were specified along an assumed streamline across the blade row. The circular-arc mean-line camber angle was obtained from the velocity-diagram entering and leaving flow angles, an assumed incidence angle, and a deviation-angle rule. Around this mean line were placed two circular-arc surfaces to produce the desired thickness at the center and the desired leading- and trailing-edge thickness. A sketch of a typical blade section is shown in figure 5. An assumed incidence angle of 4° was used for all blade sections. Recent single-stage data indicate that this incidence angle may be too low at the tip for the high tip Mach number employed. These data indicate that the incidence angle for minimum drag increases with increasing Mach number, and the drag increases rapidly as the incidence angle is decreased. The deviation-angle rule used, obtained from preliminary single-transonic-stage data, was

$$\delta^\circ = 0.475\varphi/\sigma$$

Hence, from the geometry of the blade section

$$\varphi = \Delta\beta' - i + \delta^\circ$$

or

$$\varphi = (\Delta\beta' - i)/(1 - 0.475/\sigma)$$

The solidity is obtained from a selected chord and the number of blades. It was believed desirable to obtain a high solidity in transonic rotors (ref. 7), and a solidity of approximately 1.2 at the tip and 1.88 at the hub was used for the first rotor. The high tip solidity necessitated a larger chord at the tip than at the hub.

When the included angle of the mean line is determined, together with the maximum thickness and the leading- and trailing-edge radii, the blade profile can be calculated from the circular-arc geometry of the blade section. Also, from the inlet flow angle and selected incidence angle, the angle setting of the blade section with respect to the compressor axis ψ can be determined.

Blade-section profiles were thus determined along five meridional streamline surfaces of revolution. These streamlines were assumed to pass through area centers of equal-area increments. The five sections were then stacked about a radial line passing through the approximate center of gravity of each section, and smooth surfaces were faired between sections. In order to fabricate the blade, the blade-section coordinates had to be obtained in a plane perpendicular to the radial stacking line. This was done by laying out the stacked sections to a large scale and determining the profile coordinates in a plane perpendicular to the stacking line by graphical methods.

The maximum blade thickness of the first rotor was varied from 9.5 percent of chord at the hub to 5 percent at the tip in an approximate parabolic distribution in order to reduce the blade stresses at the root. A leading- and trailing-edge radius of 0.020 inch was used for all sections. Additional blade data are given in table III.

The stator blades for the transonic stages used 65-series blower blade sections since all Mach numbers entering these stators were below 0.80 and these blade sections are known to perform well below the force-break Mach number. The blade sections were chosen in the same manner as the other subsonic blade sections.

Subsonic blades. - NACA 65-series blower blade sections were used for all subsonic blading because extensive and reliable cascade data were available for these sections and they are known to give good performance below force-break Mach numbers. The design blade camber and angle of attack for the various sections were determined from the cascade data of reference 10 for the design effective turning angle, the effective inlet air angle, and the solidity. The values of inlet air angle and turning angle given in table II for the subsonic stages are "effective angles" (fig. 3(b) of ref. 4) based on the average axial velocity across a blade row. The angles given for the transonic stages are actual angles. The blade sections for all the blade rows except the sixth, seventh, and eighth stator and exit vanes were chosen from the design charts of reference 10 (fig. 111). This choice resulted in variable camber blades, from hub to tip, set to operate at the cascade design point. In the case of the sixth, seventh, and eighth stator and exit vanes, the design-point cambers varied so little from hub to tip that a constant camber blade was used; the mean-radius design-point camber was used over the blade height. The angle of attack for the radii other than the mean was then adjusted to give the design turning angle.

No attempt was made to select camber and angle of attack off the cascade design point in order to favor part-speed performance because it was believed that this procedure would probably have an adverse effect upon the design-speed performance, and it would not be possible to determine how much the part-speed performance was improved because no comparative data would be available. The rotor blades were of constant chord length and the thickness varied from hub to tip (table III). The rotor blades were made thinner at the tip because it has been shown (ref. 1) that thin blades have high force-break Mach numbers and lower drag, and the taper in thickness also reduces the centrifugal stress in the blades. The number of blades in each blade row was determined from the desired solidity and the selected chord. The chords of the rotor blades were determined from the limiting space between stator rows which was fixed by the use of the existing casing.

3018

The number of blades in each blade row, and hence the solidity, was chosen to obtain a good operating range without undue losses. For a given design turning angle and inlet air angle, with 65-series blades, the camber necessary decreases with increasing solidity (ref. 10, fig. 109). This decrease becomes less pronounced at very high solidities. The low drag operating range also increases with decreasing camber (ref. 10, fig. 86) and hence, from a range standpoint, it is desirable to maintain high solidities. However, the total losses across a blade row will increase directly with the number of blades, and hence solidity, for fixed chord blades. A judicious selection of the number of blades and solidity is necessary in order not to penalize either the operating range or the efficiency.

In selecting the blade-section cambers and angles of attack, an interpolation was made for inlet air angle directly from the design charts, and an interpolation for solidity was made by using the design charts for three different solidities and cross-plotting these values to determine the camber and angle of attack at the chosen solidity. This procedure was also used for the variable camber stator blades. All subsonic blade sections were chosen on a "straight-through" basis; that is, the turning angle was the difference between the inlet and the outlet air angle at the same radius. The camber of such a blade section along a streamline will be somewhat lower than that of a constant-radius section, but the design turning along a streamline is also lower so that little error is involved in using the straight-through method.

The stator blades were made 6-percent thick at all radii because the thinner blade sections have higher critical Mach numbers and lower drag than the 10-percent-thick blades, and the added strength of the thicker blades is not needed because no centrifugal stresses are involved.

SUMMARY OF DESIGN CHARACTERISTICS

The various design characteristics determined in the design procedure are as follows (values given are for standard sea-level inlet conditions):

Over-all total-pressure ratio	10.26
Average stage total-pressure ratio	1.338
Weight flow, lb/sec	65
Weight flow per unit rotor frontal area, (lb/sec)/sq ft	29.8
Tip speed, ft/sec	1168
Tip speed, rpm	13,380
Over-all adiabatic efficiency	0.862

Values of total and tip static-pressure ratio per stage are plotted in figure 6. The ratio of tip static pressure to total pressure at the compressor inlet at each station is shown in figure 7(a); total-pressure ratios are given in figure 7(b).

Dimensionless axial velocity h and axial Mach number at the mean radius at each station are shown in figure 8. The distribution of dimensionless axial velocity across the annulus entering each blade row is shown in figure 9. Figure 9(a) represents the dimensionless axial velocity at the entrance to each rotor row and figure 9(b), at the entrance to each stator row.

A summary of the velocity-diagram data is given in table II for both the rotor and stator rows for five equally spaced radial stations at the rotor and stator entrance. Values of the diffusion factors (D or D') are listed for tip, mean, and hub radii.

A summary of the blade design data is given in table III; the number of blades, blade chord, solidity, camber, maximum thickness, and section setting angle are listed for various radii.

OVER-ALL TEST RESULTS

The compressor was tested in accordance with the standard procedure of reference 11. Performance characteristics determined experimentally are presented in figure 10. The experimentally determined performance shown in figure 10 is discussed in detail in reference 12.

National Advisory Committee for Aeronautics
Lewis Flight Propulsion Laboratory
Cleveland, Ohio, September 30, 1953

3018

CS-3 back

[redacted]

REFERENCES

1. Bogdonoff, Seymour M.: NACA Cascade Data for the Blade Design of High-Performance Axial-Flow Compressors. Jour. Aero Sci., vol. 15, no. 2, Feb. 1948, pp. 89-95.

2. Dugan, Paul D., Mahoney, John J., and Benser, William A.: Effect of Mach Number on Performance of an Axial-Flow Compressor Rotor-Blade Row. NACA RM E8D29, 1948.

3. Voit, Charles H., Guentert, Donald C., and Dugan, James F.: Effect of Mach Number on Over-All Performance of Single-Stage Axial-Flow Compressor Designed for High Pressure Ratio. NACA RM E50D26, 1950.

4. Johnsen, Irving A.: Investigation of a 10-Stage Subsonic Axial Flow Compressor. I - Aerodynamic Design. NACA RM E52B18, 1952.

5. Budinger, Ray E., and Thomson, Arthur R.: Investigation of a 10-Stage Subsonic Axial-Flow Research Compressor. II - Preliminary Analysis of Over-All Performance. NACA RM E52C04, 1952.

6. Voit, Charles H., and Thomson, Arthur R.: An Analytical Investigation Using Aerodynamic Limitations of Several Designs of High Stage Pressure Ratio Multistage Compressors. NACA TN 2589, 1951.

7. Lieblein, Seymour, Lewis, George W., Jr., and Sandercock, Donald M.: Experimental Investigation of an Axial-Flow Compressor Inlet Stage Operating at Transonic Relative Inlet Mach Numbers. I - Over-All Performance of Stage with Transonic Rotor and Subsonic Stators up to Rotor Relative Inlet Mach Numbers of 1.1. NACA RM E52A24, 1952.

8. Lieblein, Seymour, Schwenk, Francis C., and Broderick, Robert L.: Diffusion Factor for Estimating Losses and Limiting Blade Loadings in Axial-Flow-Compressor Blade Elements. NACA RM E53D01, 1953.

9. Burtt, Jack R.: Investigation of Performance of Typical Inlet Stage of Multistage Axial-Flow Compressor. NACA RM E9E13, 1949.

10. Herrig, L. Joseph, Emery, James C., and Erwin, John R.: Systematic Two-Dimensional Cascade Tests of NACA 65-Series Compressor Blades at Low Speeds. NACA RM L51G31, 1951.

11. NACA Subcommittee on Compressors: Standard Procedures for Rating and Testing Multistage Axial-Flow Compressors. NACA TN 1138, 1946.

12. Geye, Richard P., Budinger, Ray E., and Voit, Charles H.: Investigation of a High-Pressure-Ratio Eight-Stage Axial-Flow Research Compressor with Two Transonic Inlet Stages. II - Preliminary Analysis of Over-All Performance. NACA RM E53J06, 1953.

3018

3018

TABLE I. - DESIGN DATA

Stage	Stage total-pressure ratio	Tip dimensionless axial-velocity ratio entering stage	Tip relative inlet air angle entering stage	Assumed stage polytropic efficiency
Subsonic stages				
1	1.189	0.3855	60.00	0.81
2	1.251	.4015	59.00	.86
3	1.291	.4178	58.00	.91
4	1.322	.4360	57.01	.91
5	1.343	.4570	56.03	.91
6	1.349	.4815	55.08	.91
7	1.340	.5000	54.16	.91
8	1.312	.5000	53.30	.88
9	1.278	.5000	52.50	.85
Transonic stages				
1	1.374	0.4963	63.61	0.88
2	1.374	.4936	59.84	.88

3018

TABLE II. - VECTOR-DIAGRAM DATA

(a) Rotor.

Stage	Axial station	Entrance							Change through blade row		D'
		Z	X	Y'	h	V'/U_t	M'	β'	Δh	Δβ'	
1	1	1.0000	0	0.2462	0.4963	1.116	1.201	63.61	-0.0169	6.07	0.285
		.8700	0	.2696	.4963	1.002	1.078	61.11	-.0169	7.79	-----
		.7400	0	.3012	.4963	.8912	.959	57.68	-.0169	10.57	.371
		.6100	0	.3474	.4963	.7867	.8465	52.65	-.0169	15.65	-----
		.4800	0	.4274	.4963	.6905	.743	44.05	-.0169	26.09	.433
2	3	1.0000	0.1505	0.2728	0.4936	0.9824	1.0036	59.84	-0.0047	10.13	0.330
		.9026	.1505	.2973	.4960	.9008	.9208	56.68	-.0110	12.82	-----
		.8052	.1505	.3261	.4986	.8228	.8409	52.65	-.0192	16.58	.396
		.7073	.1505	.3602	.5015	.7492	.7656	48.02	-.0308	21.82	-----
		.6103	.1505	.4067	.5049	.6830	.6984	42.32	-.0484	31.28	.449
3	5	1.0000	0.3314	0.2352	0.4178	0.7884	0.7610	58.75	-0.0242	11.86	0.414
		.9200	.3049	.2556	.4564	.7659	.7404	53.62	-.0112	15.20	-----
		.8400	.2784	.2800	.4891	.7447	.7208	48.71	.0001	18.98	.398
		.7600	.2519	.3095	.5170	.7249	.7026	43.89	.0112	18.98	-----
		.6800	.2254	.3459	.5410	.7067	.6838	39.14	.0225	28.12	.347
4	7	1.0000	0.3283	0.2794	0.4360	0.8008	0.7428	57.57	-0.0186	14.98	0.443
		.9343	.3068	.2991	.4664	.7819	.7255	53.44	-.0070	18.20	-----
		.8686	.2852	.3217	.4930	.7638	.7095	49.50	.0030	21.79	.422
		.8029	.2636	.3480	.5164	.7467	.6943	45.62	.0131	25.70	-----
		.7372	.2421	.3790	.5371	.7305	.6803	41.50	.0234	29.78	.380
5	9	1.0000	0.3217	0.3226	0.4570	0.8179	0.7255	56.37	-0.0117	18.22	0.470
		.9464	.3045	.3409	.4800	.8016	.7112	53.18	-.0024	21.12	-----
		.8928	.2872	.3613	.5008	.7859	.6978	50.06	.0062	24.34	.454
		.8392	.2700	.3844	.5197	.7708	.6850	46.49	.0141	27.33	-----
		.7856	.2527	.4106	.5367	.7564	.6731	43.92	.0230	31.46	.419
6	11	1.0000	0.3103	0.3598	0.4815	0.8411	0.7111	55.35	-0.0098	20.66	0.506
		.9570	.2970	.3759	.4980	.8269	.6993	52.96	-.0023	23.26	-----
		.9140	.2836	.3936	.5134	.8130	.6881	50.58	.0047	26.02	.490
		.8710	.2703	.4130	.5276	.7994	.6770	48.21	.0119	28.94	-----
		.8280	.2569	.4345	.5407	.7865	.6663	45.87	.0186	32.02	.465
7	13	1.0000	0.2860	0.3850	0.5000	0.8717	0.7029	55.36	-0.0132	21.66	0.523
		.9650	.2759	.3989	.5111	.8580	.6920	53.57	-.0069	23.86	-----
		.9300	.2659	.4139	.5216	.8445	.6815	51.77	-.0005	26.22	.515
		.8950	.2559	.4301	.5315	.8312	.6710	49.97	.0058	28.70	-----
		.8600	.2459	.4476	.5409	.8184	.6609	48.63	.0115	31.77	.499
8	15	1.0000	0.2860	0.4022	0.5000	0.8717	0.6717	55.29	-0.0108	23.06	0.542
		.9712	.2777	.4142	.5092	.8603	.6631	53.81	-.0049	24.97	-----
		.9424	.2695	.4268	.5180	.8492	.6547	52.34	.0008	26.99	.533
		.9136	.2612	.4403	.5263	.8382	.6465	50.85	.0065	29.05	-----
		.8848	.2530	.4546	.5343	.8275	.6384	49.34	.0122	31.26	.521

3018

TABLE II. - Concluded. VECTOR-DIAGRAM DATA

(b) Stator.

Stage	Axial station	Entrance							Change through blade row		D
		Z	X	Y	h	V/U_t	M	β	Δh	Δβ	
1	2	1.0000	0.2462	0.0957	0.4794	0.5390	0.5520	27.18	0.0142	10.22	0.152
		.9133	.2696	.1191	.4794	.5501	.5641	29.35	.0166	12.45	-----
		.8174	.3012	.1507	.4794	.5663	.5817	32.14	.0192	15.32	.209
		.7087	.3474	.1969	.4794	.5921	.6103	35.93	.0221	19.20	-----
		.5761	.4274	.2769	.4794	.6423	.6663	41.71	.0255	25.11	.329
2	4	1.0000	0.4233	0.0919	0.4889	0.6467	0.6351	40.89	-0.0711	2.47	0.247
		.9136	.4473	.1422	.4850	.6600	.6488	42.63	-.0286	8.92	-----
		.8273	.4762	.1980	.4794	.6758	.6660	44.83	.0097	15.18	.289
		.7409	.5117	.2595	.4707	.6948	.6870	47.37	.0463	21.38	-----
		.6545	.5572	.3318	.4565	.7203	.7143	50.67	.0845	28.05	.314
3	6	1.0000	0.5666	0.2383	0.3936	0.6899	0.6522	53.79	0.0424	15.43	0.179
		.9273	.5609	.2564	.4452	.7191	.6823	50.81	.0212	17.15	-----
		.8546	.5584	.2778	.4892	.7477	.7122	48.52	.0038	18.91	.259
		.7819	.5599	.3032	.5282	.7774	.7434	46.80	-.0118	20.78	-----
		.7092	.5666	.3337	.5635	.8082	.7763	45.63	-.0264	22.84	.340
4	8	1.0000	0.6077	0.2860	0.4174	0.7372	0.6688	54.27	0.0396	17.92	0.304
		.9405	.6059	.3033	.4594	.7629	.6942	52.15	.0206	19.43	-----
		.8810	.6065	.3231	.4960	.7881	.7194	50.87	.0048	21.35	.358
		.8215	.6098	.3455	.5295	.8140	.7457	49.14	-.0098	22.53	-----
		.7620	.6169	.3717	.5605	.8413	.7736	48.17	-.0238	24.23	.414
5	10	1.0000	0.6443	0.3340	0.4453	0.7832	0.6796	54.28	0.0362	20.47	0.384
		.9520	.6447	.3493	.4776	.8045	.6997	52.85	.0204	21.70	-----
		.9040	.6476	.3671	.5070	.8264	.7208	51.68	.0064	22.96	.421
		.8560	.6523	.3867	.5338	.8487	.7423	50.74	-.0062	24.25	-----
		.8080	.6592	.4085	.5597	.8715	.7645	50.00	-.0190	25.62	.460
6	12	1.0000	0.6701	0.3841	0.4717	0.8195	0.6785	54.05	0.0283	23.57	0.458
		.9613	.6725	.3976	.4957	.8370	.6945	53.15	.0154	24.54	-----
		.9226	.6762	.4124	.5181	.8548	.7107	52.39	.0035	25.53	.482
		.8839	.6813	.4285	.5395	.8733	.7276	51.75	-.0080	26.55	-----
		.8452	.6880	.4463	.5593	.8916	.7446	51.26	-.0184	27.61	.507
7	14	1.0000	0.6710	0.3850	0.4868	0.8290	0.6540	53.67	0.0132	23.58	0.461
		.9684	.6744	.3975	.5042	.8431	.6660	53.27	.0050	24.63	-----
		.9368	.6788	.4109	.5211	.8580	.6789	52.53	-.0031	25.29	.480
		.9052	.6841	.4253	.5373	.8730	.6919	52.08	-.0110	26.18	-----
		.8736	.6905	.4407	.5524	.8881	.7050	51.72	-.0181	27.09	.500
8	16	1.0000	0.6882	0.4022	0.4892	0.8443	0.6363	54.30	0.0108	24.27	0.486
		.9732	.6916	.4123	.5043	.8566	.6463	53.79	.0038	25.00	-----
		.9464	.6956	.4250	.5188	.8690	.6564	53.34	-.0030	25.75	.499
		.9244	.7004	.4374	.5328	.8819	.6670	52.95	-.0096	26.50	-----
		.8992	.7058	.4505	.5465	.8954	.6782	52.62	-.0161	27.29	.514

TABLE III. - BLADE DESIGN DATA

(a) Rotor.

Stage	Radius ratio, Z	Number of blades	Blade chord, in.	Solidity	Design camber, $C_{L,i}$	Design camber, φ, deg	Thickness, percent of chord	Angle setting, ψ, deg
1	1.0000	20	3.766	1.186	----	2.09	5.0	58.54
	.8990		3.675	1.280	----	4.85	5.4	54.67
	.7840		3.528	1.396	----	9.19	5.9	49.01
	.6500		3.291	1.549	----	17.06	7.1	40.12
	.4800		3.015	1.864	----	33.75	9.5	23.17
2	1.0000	23	3.50	1.281	----	6.58	4.8	52.55
	.9233		3.385	1.332	----	9.14	5.2	48.61
	.8398		3.188	1.392	----	13.12	5.8	43.30
	.7465		2.997	1.473	----	19.40	6.7	35.76
	.6318		2.791	1.618	----	31.06	8.6	22.97
3	1.0000	41	1.46	0.953	0.82	-----	6.0	49.5
	.9200		1.46	1.036	.94	-----	7.0	42.9
	.8400		1.46	1.134	1.09	-----	8.0	36.3
	.7600		1.46	1.254	1.24	-----	9.0	29.6
	.6800		1.46	1.401	1.39	-----	10.0	22.5
4	1.0000	49	1.42	1.107	0.93	-----	6.0	46.6
	.8686		1.42	1.275	1.18	-----	8.0	35.6
	.7372		1.42	1.502	1.44	-----	10.0	23.8
5	1.0000	53	1.37	1.156	1.10	-----	6.0	43.8
	.8928		1.37	1.294	1.33	-----	7.0	34.7
	.7856		1.37	1.471	1.58	-----	8.0	25.2
6	1.0000	54	1.31	1.126	1.28	-----	6.0	41.5
	.9140		1.31	1.232	1.49	-----	7.0	34.4
	.8280		1.31	1.360	1.71	-----	8.0	26.9
7	1.0000	55	1.28	1.120	1.35	-----	6.0	41.0
	.9300		1.28	1.205	1.54	-----	7.0	35.3
	.8600		1.28	1.303	1.73	-----	8.0	29.4
8	1.0000	57	1.23	1.116	1.45	-----	6.0	40.2
	.9424		1.23	1.184	1.62	-----	7.0	35.3
	.8848		1.23	1.261	1.77	-----	8.0	30.5

TABLE III. - Concluded. BLADE DESIGN DATA

(b) Stator.

Stage	Radius ratio, Z	Number of blades	Blade chord, in.	Solidity	Design camber, $C_{L,i}$	Thickness, percent of chord	Angle setting, ψ, deg
1	1.0000	27	1.900	0.817	0.58	6.0	20.0
	.8941		1.900	.913	.69	6.0	21.3
	.7881		1.900	1.036	.83	6.0	22.7
	.6821		1.900	1.197	.98	6.0	24.4
	.5761		1.900	1.417	1.16	6.0	26.3
2	1.0000	32	1.950	0.993	0.34	6.0	37.1
	.9136		1.950	1.087	.54	6.0	35.5
	.8273		1.950	1.200	.76	6.0	34.2
	.7409		1.950	1.340	.97	6.0	33.2
	.6545		1.950	1.517	1.19	6.0	32.5
3	1.0000	33	1.460	0.767	1.23	6.0	43.0
	.9273		1.460	.827	1.26	6.0	39.3
	.8546		1.460	.897	1.30	6.0	36.1
	.7819		1.460	.981	1.32	6.0	33.6
	.7092		1.460	1.081	1.36	6.0	31.5
4	1.0000	35	1.420	0.791	1.41	6.0	42.0
	.8810		1.420	.898	1.46	6.0	36.9
	.7620		1.420	1.038	1.51	6.0	33.1
5	1.0000	39	1.380	0.857	1.58	6.0	41.9
	.9040		1.380	.948	1.58	6.0	37.0
	.8080		1.380	1.060	1.58	6.0	32.7
6	1.0000	43	1.32	0.903	1.70	6.0	39.9
	.9230		1.32	.979	1.70	6.0	36.3
	.8450		1.32	1.069	1.70	6.0	33.2
7	1.0000	46	1.28	0.937	1.70	6.0	39.5
	.9370		1.28	1.000	1.70	6.0	36.7
	.8740		1.28	1.073	1.70	6.0	34.2
8	1.0000	49	1.23	0.959	1.70	6.0	39.5
	.9460		1.23	1.014	1.70	6.0	37.1
	.8930		1.23	1.074	1.70	6.0	34.8

3018

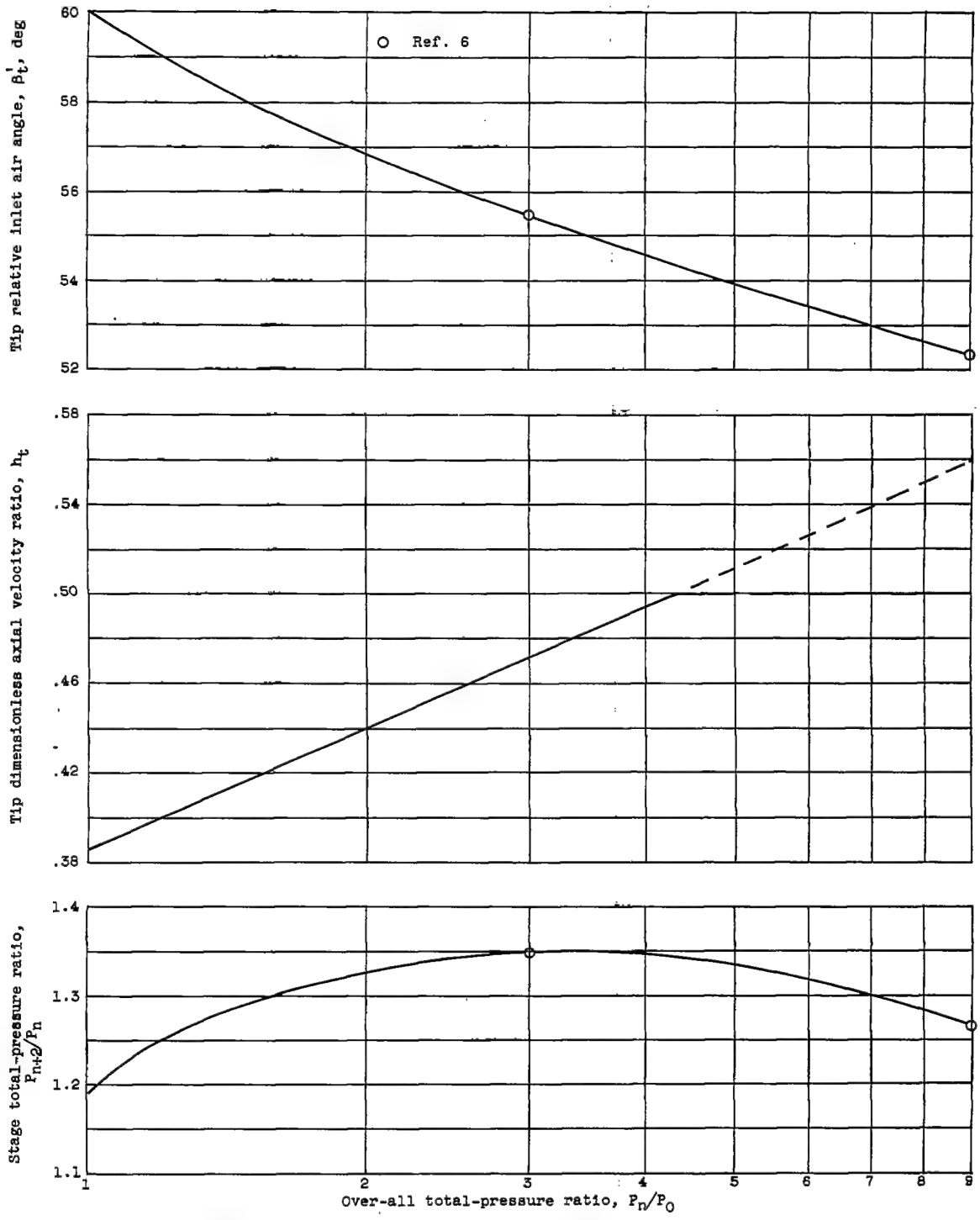

Figure 1. - Stagewise distribution of stage total-pressure ratio, dimensionless axial velocity, and tip relative inlet air angle.

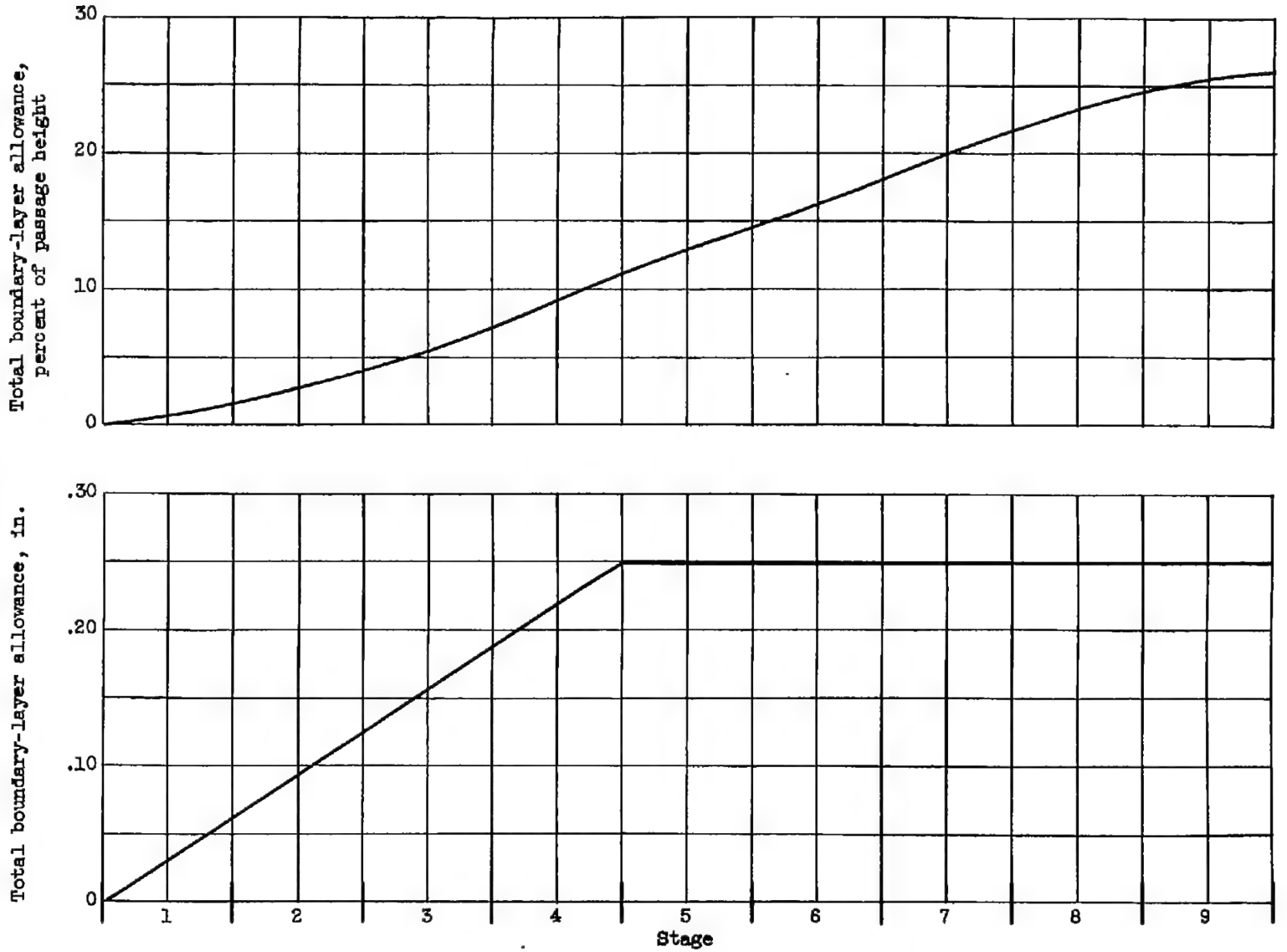

Figure 2. - Stagewise distribution of boundary-layer allowance.

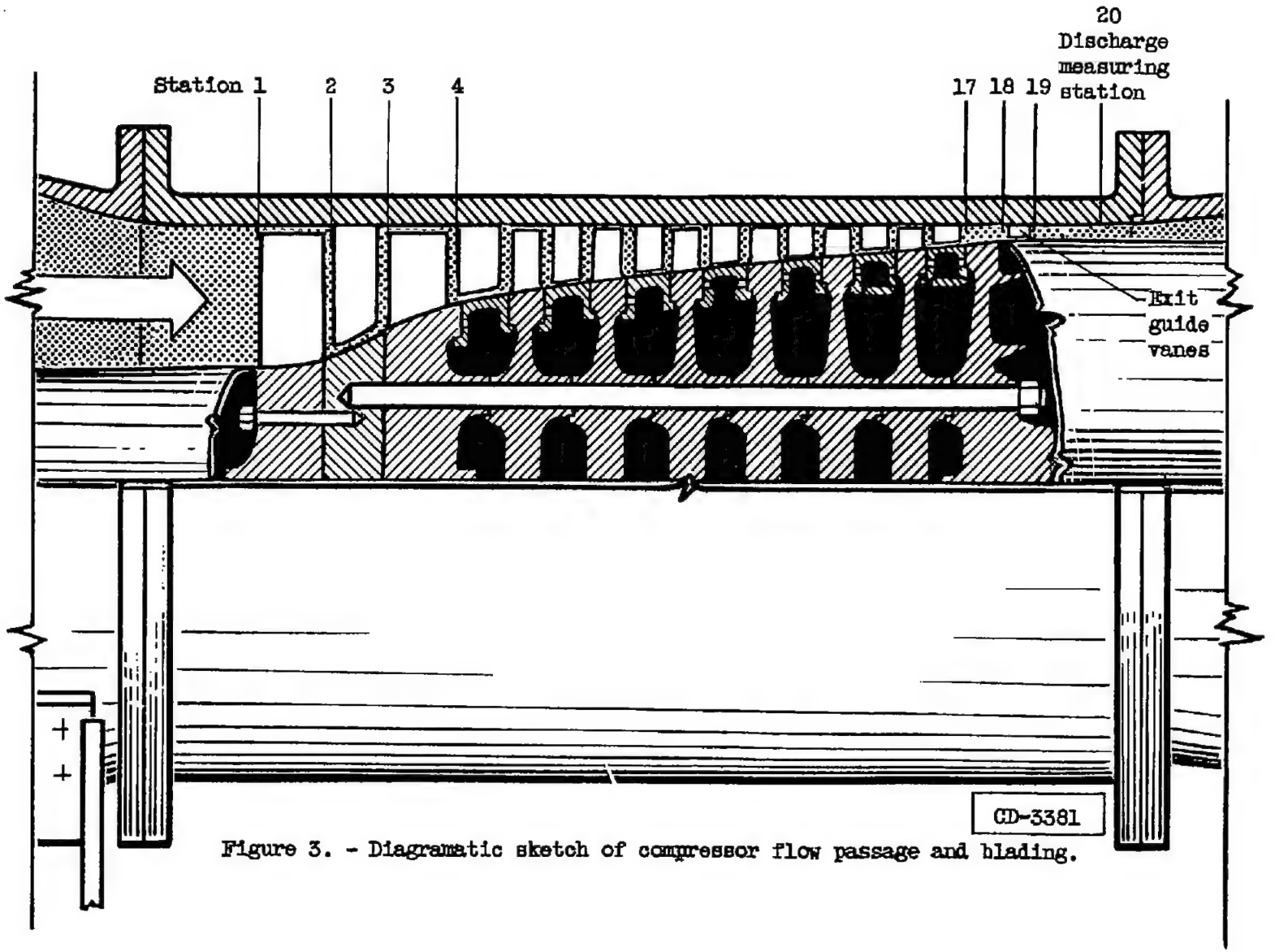

Figure 3. - Diagramatic sketch of compressor flow passage and blading.

3018

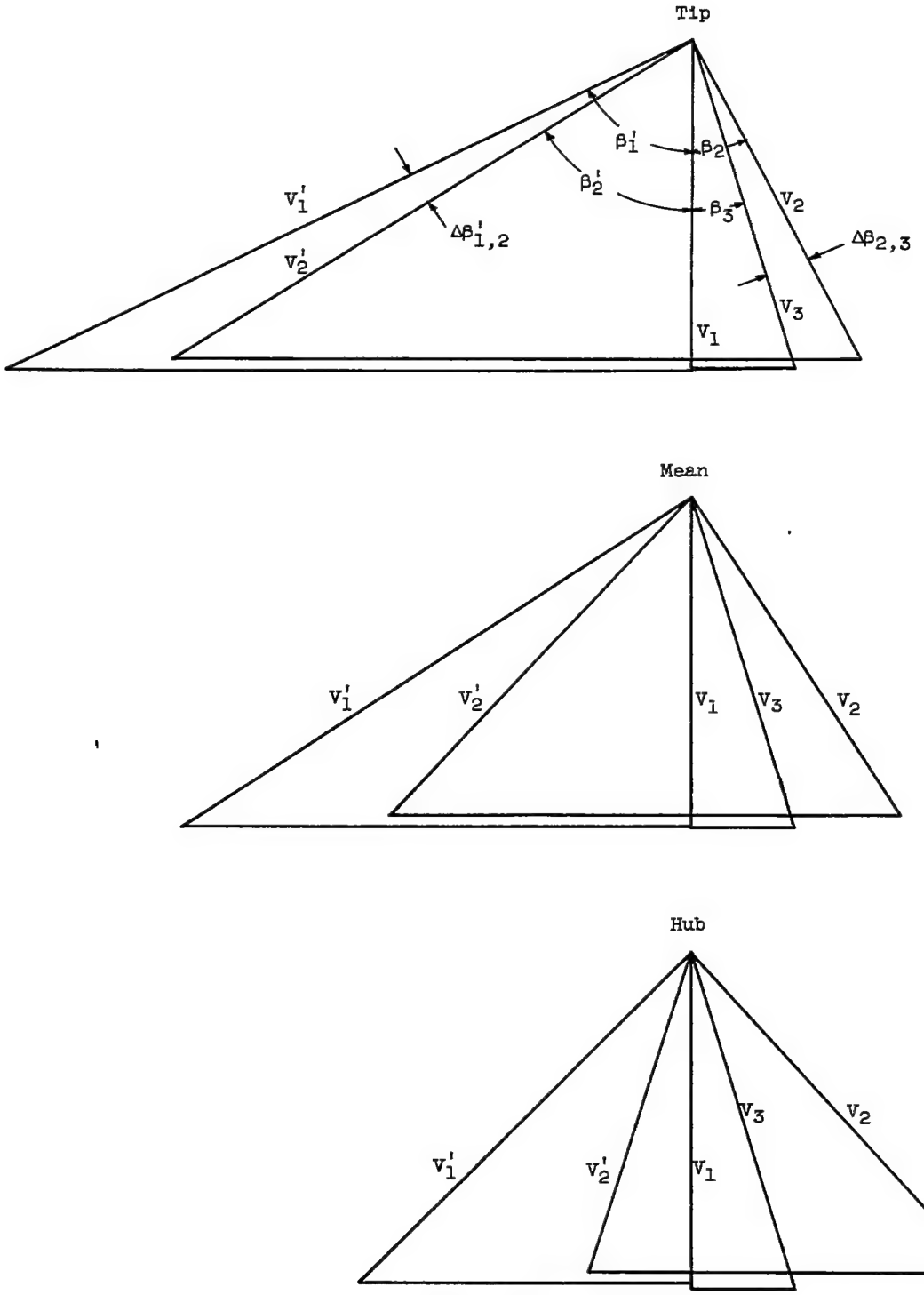

(a) First stage.

Figure 4. - Velocity diagrams for stages at tip, mean, and hub radii.

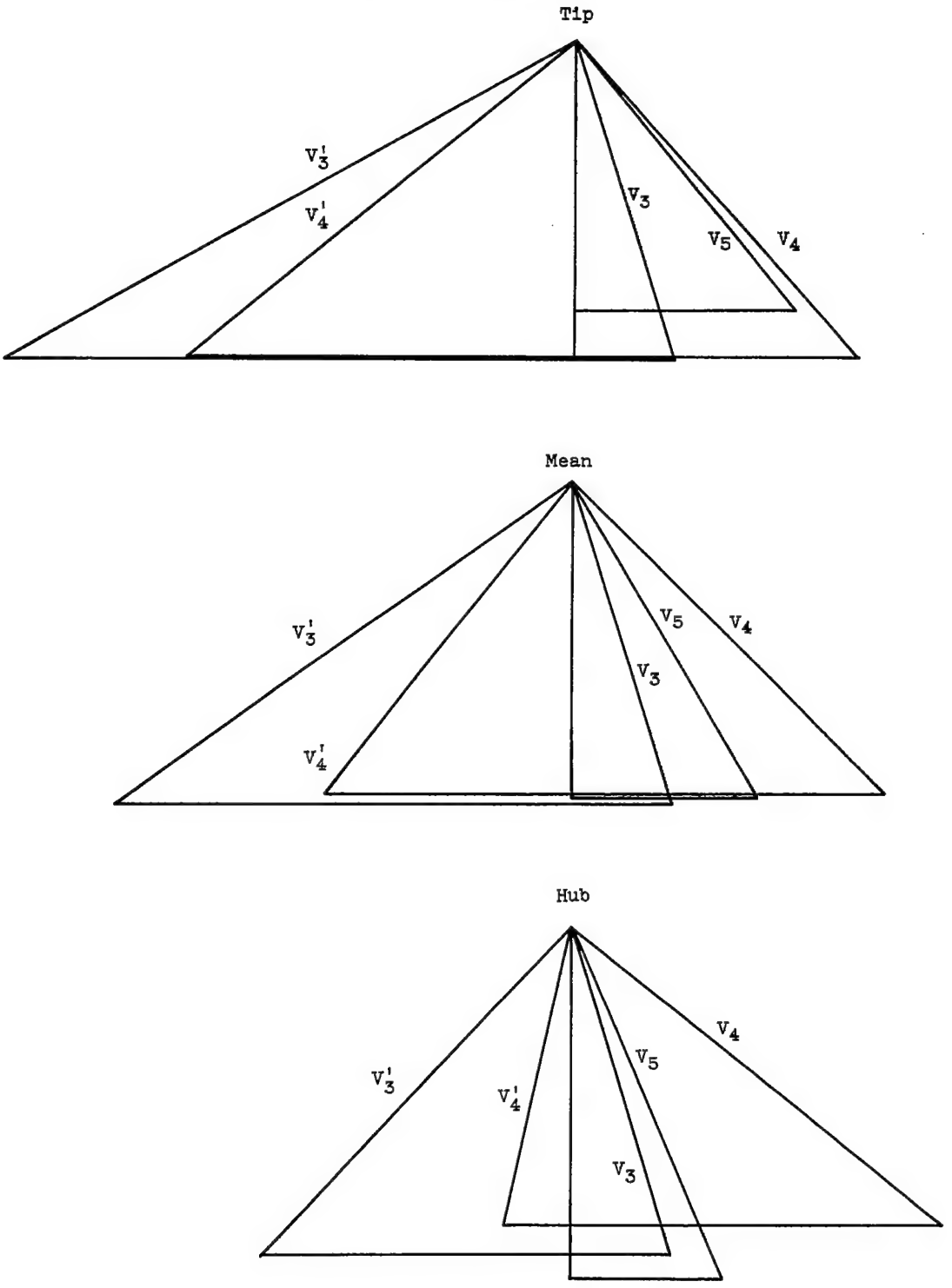

(b) Second stage.

Figure 4. - Concluded. Velocity diagrams for stages at tip, mean, and hub radii.

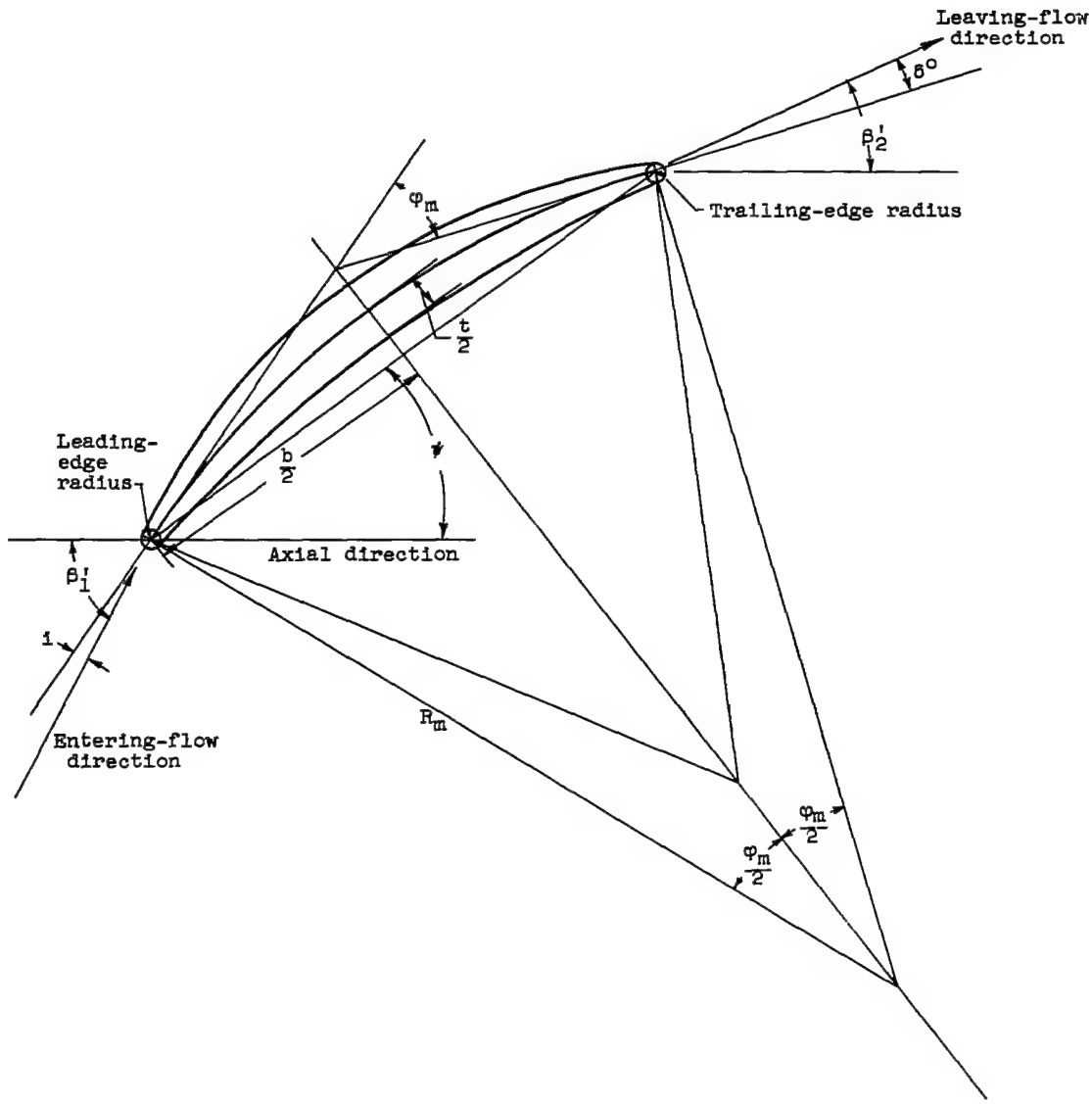

Figure 5. - Typical transonic blade section.

3018

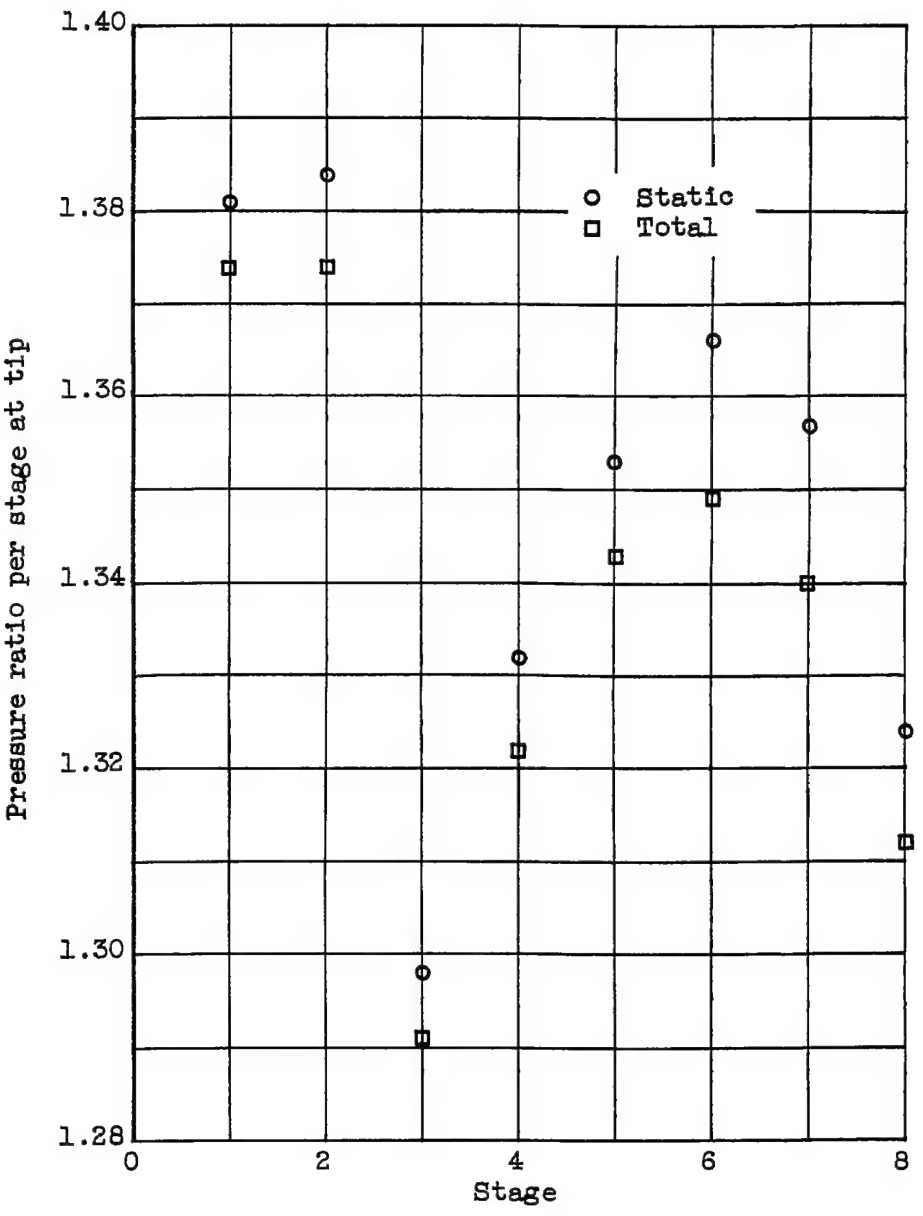

Figure 6. - Variation of design stage pressure ratio.

3018

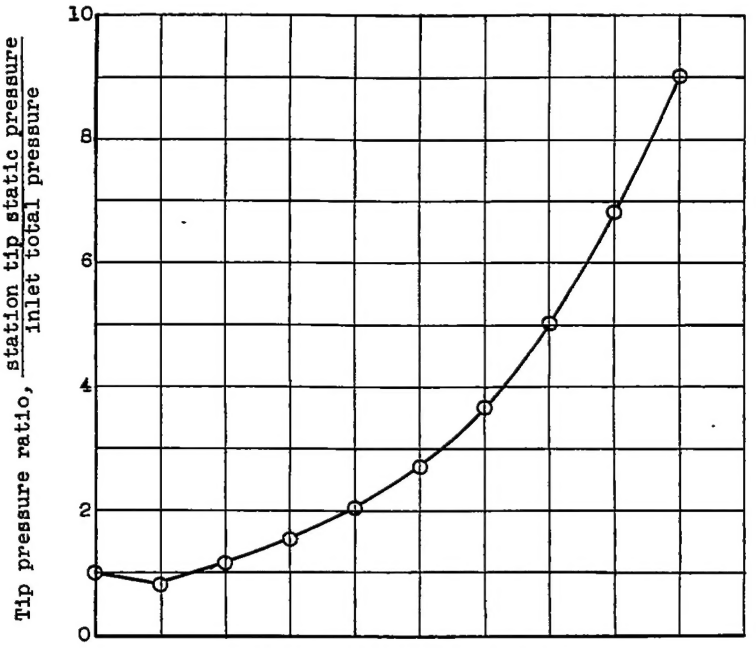

(a) Tip static pressure.

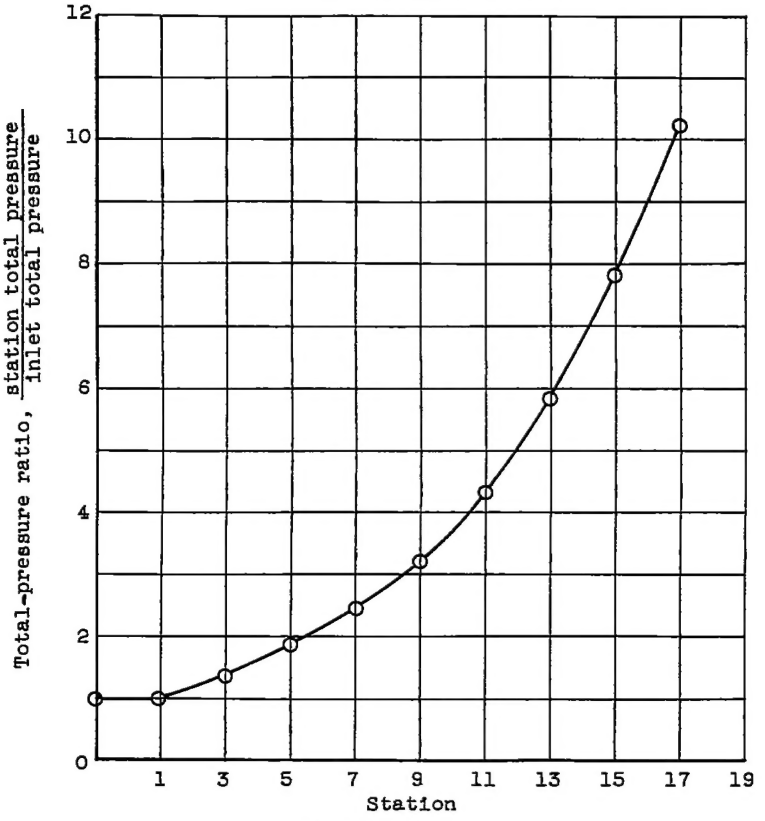

(b) Total pressure.

Figure 7. - Design pressure ratio thrcugh compressor.

[redacted]

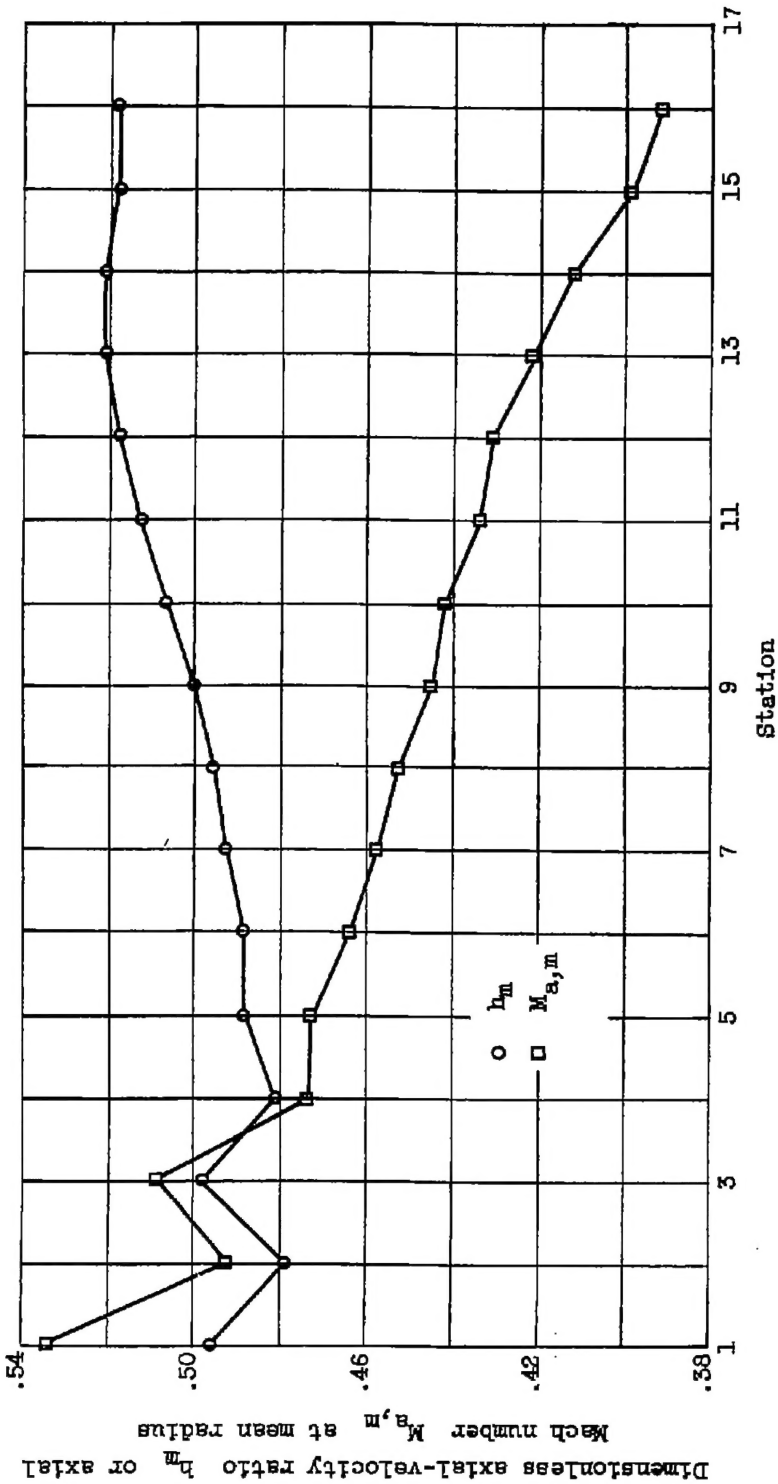

Figure 8. - Variation of dimensionless axial-velocity ratio and axial Mach number through compressor.

3018

3018

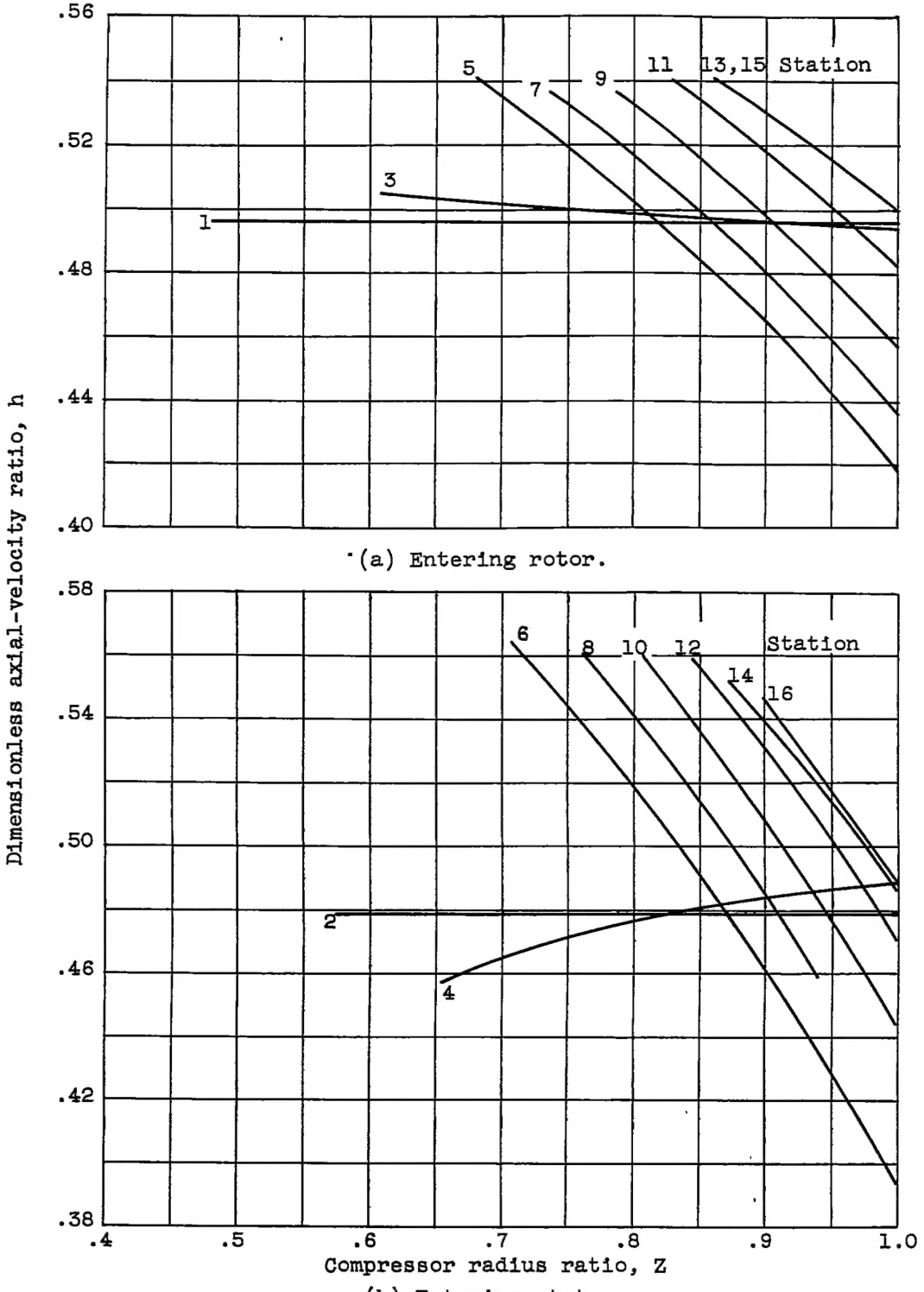

Figure 9. - Radial distribution of dimensionless axial-velocity ratio.

CONFIDENTIAL

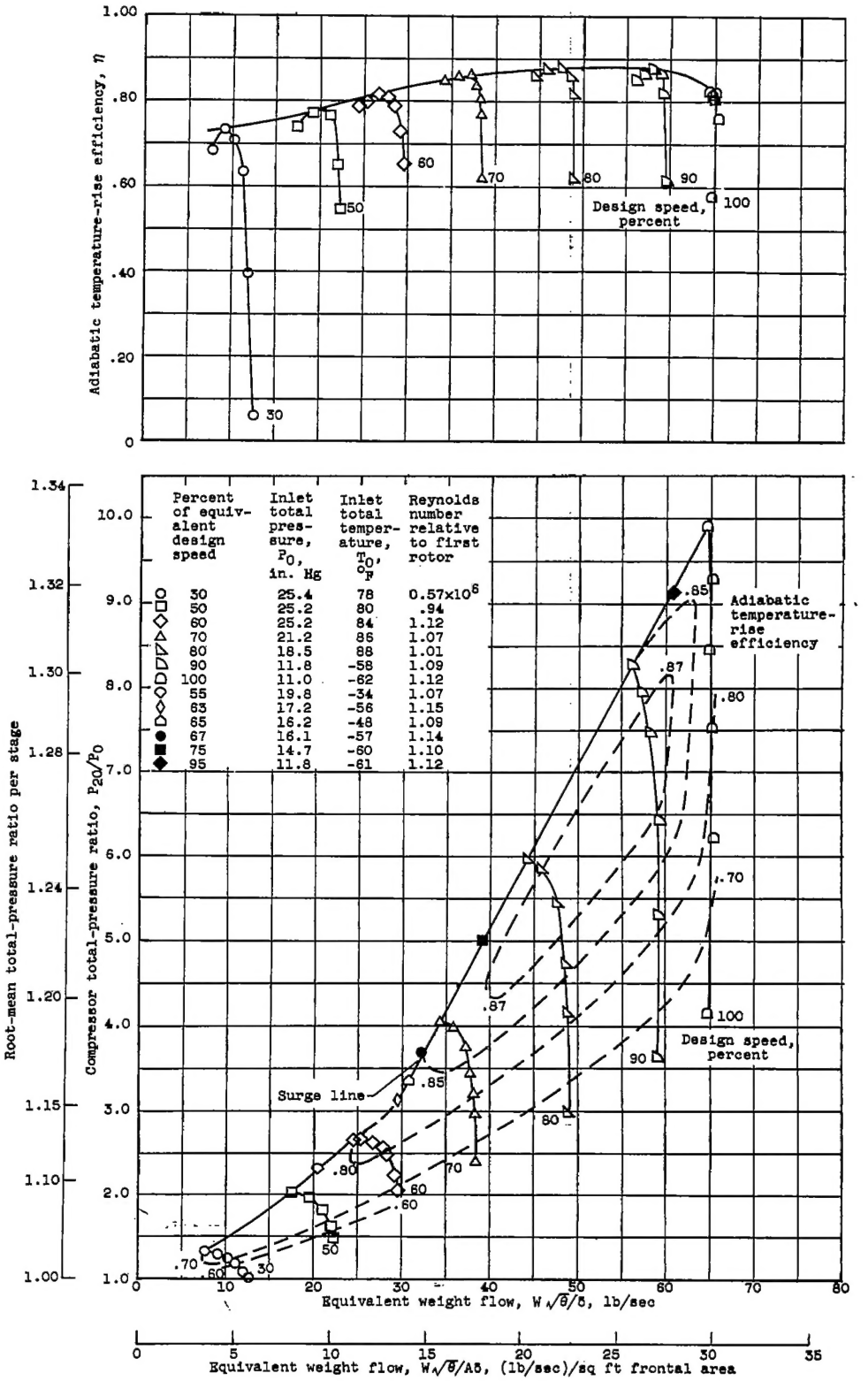

Figure 10. - Over-all performance characteristics of eight-stage axial-flow compressor.